Bartholazzi, Gabriel; Jussila, Topias; Obenlüneschloß, Jorit; Vähänissi, Ville; Devi, Anjana; Savin, Hele; Karppinen, Maarit; Macdonald, Daniel H.; Black, Lachlan E.

Atomic-layer-deposited CuxCryOz thin films: Optoelectronic properties and potential application as hole-selective contacts for c-Si solar cells

Published in:
Applied Surface Science

DOI:
10.1016/j.apsusc.2024.161793

Published: 28/02/2025

Document Version
Publisher's PDF, also known as Version of record

Applied Surface Science 683 (2025) 161793

Contents lists available at ScienceDirect

Applied Surface Science

journal homepage: www.elsevier.com/locate/apsusc

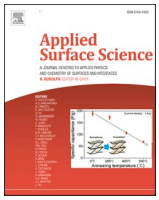

Full Length Article

Atomic-layer-deposited $Cu_xCr_yO_z$ thin films: Optoelectronic properties and potential application as hole-selective contacts for c-Si solar cells

Gabriel Bartholazzi [a,*], Topias Jussila [b], Jorit Obenlüneschloß [c], Ville Vähänissi [d], Anjana Devi [c,e,f], Hele Savin [d], Maarit Karppinen [b], Daniel H. Macdonald [a], Lachlan E. Black [a]

[a] School of Engineering, the Australian National University, 2600 Canberra, Australia
[b] Department of Chemistry and Materials Science, Aalto University, FI-00076 Aalto, Finland
[c] Inorganic Materials Chemistry, Ruhr University Bochum, 44801 Bochum, Germany
[d] Department of Electronics and Nanoengineering, Aalto University, Tietotie 3, 02150 Espoo, Finland
[e] Leibniz Institute for Solid State and Materials Research, IFW Dresden, 01069 Dresden, Germany
[f] Chair of Materials Chemistry, TU Dresden, 01069 Dresden, Germany

ARTICLE INFO

Keywords:
Copper chromium oxide
Atomic layer deposition
Hole-selective materials
Optoelectronic properties
Band diagram

ABSTRACT

In this work, we investigate the properties of $Cu_xCr_yO_z$ thin films deposited by atomic layer deposition (ALD) over a wide compositional range. A significant increase in growth rate is observed for intermediate compositions and shown to arise from an enhancement of the CrO_x deposition rate on the CuO_x surface. In addition to the characteristics of the deposition process, we explore the structural and optoelectronic properties of these films for compositions ranging from copper-free chromium oxide to chromium-free copper oxide, and for various post-deposition annealing temperatures (400–800 °C). The resulting composition, optical constants, band gap, valence band maximum and work function are determined and used to draw full band diagrams of the binary and ternary oxides. We report for the first time the experimental work function of the spinel phase $CuCr_2O_4$ (5.0 ± 0.2 eV). Finally, the contact resistivity of the films with p-type silicon is examined to assess their potential use as hole-selective contacts for crystalline Si solar cells. The lowest contact resistivity (1.72 Ω cm^2) was found for as-deposited $Cu_{0.05}Cr_{0.30}O_{0.65}$.

1. Introduction

Transparent conductive oxide (TCO) materials enable the development of various high-performance optoelectronic devices, including solar cells, touch screens, and LEDs [1–4]. The majority of high-performance TCOs used in industry are n-type conductors, which limits the potential of TCOs in some applications as the lack of p-type TCOs hinders, for instance, the development of heterojunctions and more efficient hole-collectors, which are essential for optoelectronic devices such as solar cells [5]. In this context, the delafossite family of materials have emerged as candidate p-type TCOs, with the potential to close the considerable gap in conductivity and transparency with their n-type counterparts [6–9]. Delafossites represent a family of ternary oxide materials with the $A^{+1}B^{+3}O_2^{-2}$ formula, where A (e.g. Ag, Cu, Pd, Pt) and B (e.g. Ga, In, Al, Fe, Cr, Eu) are metal cations [10–12]. Among this material family, Cu-based delafossites have received increasing attention since the first work that demonstrated p-type conductivity and transparency in $CuAlO_2$ [13]. Their p-type character arises from Cu vacancies in the lattice in addition to interstitial oxygen, leading to high hole-mobility [14]. Subsequently, other materials based on $Cu_xFe_yO_z$, [15,16] $Cu_xB_yO_z$, [17] $Cu_xIn_yO_z$, [18] $Cu_xGa_yO_z$, [19,20] and $Cu_xCr_yO_z$ [21–23] have also been investigated. Among these, $Cu_xCr_yO_z$ stands out due to the combination of high band gap and conductivity, low synthesis temperature, and stability in air [24]. $Cu_xCr_yO_z$ materials present two main stable phases, delafossite $CuCrO_2$ and spinel $CuCr_2O_4$. The former has been widely investigated as a potential p-type TCO in optoelectronic devices, water splitting, and energy storage [25]. It presents conductivity in the order of 102 S cm^{-1}, [26] work function of ~5.2 eV, [27] and an electron affinity of 2.29–2.50 eV [27,28]. The nature of its band gap is somewhat controversial, with direct band gaps of 2.9–3.3 eV [26,27,29–31] and even indirect transitions reported [32]. On the other hand, the spinel $CuCr_2O_4$ has been applied to catalysts, [33–35] hydrogen production, [36,37] and as a coating in concentrated solar power systems [38]. Its electrical conductivity is in the ~10^{-2} S cm^{-1}

* Corresponding author.
E-mail address: gabriel.bartholazzi@anu.edu.au (G. Bartholazzi).

https://doi.org/10.1016/j.apsusc.2024.161793
Received 11 October 2024; Received in revised form 7 November 2024; Accepted 12 November 2024
Available online 14 November 2024

range, [39] and a direct band gap of ~1.3–1.9 eV [40–42] has been reported for thin films, with one DFT study, however, describing a metallic-like behaviour (no band gap) [43]. Despite a range of work focusing on the characterization of its crystal structure, there is scarce information on its optoelectronic properties such as work function, which limits the ability to fully understand this material and to identify potential applications.

$Cu_xCr_yO_z$ thin films have been manufactured by various physical and chemical deposition methods, including sputtering, [44–46] pulsed laser deposition (PLD), [47,48] chemical vapour deposition (CVD), [49–51] molecular beam epitaxy (MBE), solution-processing, [34,39,41] and atomic layer deposition (ALD) [22,31,40,52]. Although all methods have been shown to produce stoichiometric delafossite or spinel material, very few studies have investigated the effects of tuning the composition and the resulting optoelectronic properties. Bottiglieri *et al.* reported, for a Cu-rich film, lower resistivity and a higher Gordon's figure of merit in terms of optical absorption and electrical conductivity when compared to the stoichiometric $CuCrO_2$ phase [53]. Bottiglieri *et al.* also reported a drop in band gap with increasing Cu content [49]. The authors found that a Cu-rich film, as a hole-selective material, resulted in a higher efficiency for an organic solar cell when compared to a more stoichiometric one. Both reports employed aerosol-assisted metal–organic CVD (AA-MOCVD) [49,53]. On the other hand, Xu *et al.* deposited chromium-rich thin films using spin-coating, achieving a range of work function and contact resistivity values on silicon by varying the post-deposition annealing temperature [54].

For applications where charge carrier control is important, such as carrier-selective contacts for solar cells, out-of-stoichiometric compositions may be ideal to tune the device's performance. In the case of photovoltaic devices, appropriate work function and band alignment enables a more efficient extraction of charge carriers [55,56]. Additionally, amorphous phases could minimize the presence of silicon dangling bonds, and thus reduce interfacial defects. Both CrO_x and CuO_x, as well as their combination in ternary compounds, have been investigated as potential hole-selective contacts in perovskite, organic, and silicon solar cells [54,57–61]. For the latter, only the binary oxides and a copper-doped CrO_x study have been reported [54,58,62,63].

Most studies used a solution-based process to deposit the $Cu_xCr_yO_z$ thin films, which limits the scalability of the process. In that sense, ALD – a scalable thin film deposition technique widely employed in the microelectronics industry – is the perfect tool to precisely investigate different compositions and achieve sub-nanometre control over film thickness, uniformity, and conformality due to its self-limiting surface reactions [64–67]. In our previous work, we deposited $Cu_xCr_yO_z$ films via ALD using copper 2,2,6,6-tetramethyl-3,5-heptanedionate (Cu(thd)$_2$) and chromium acetylacetonate (Cr(acac)$_3$) metal precursors and O_3 as a co-reactant, to achieve crystalline $CuCrO_2$ and $CuCr_2O_4$ phases through different rapid thermal annealing conditions [22,31,40,52]. Here we investigate in more detail the film growth characteristics of our $Cu_xCr_yO_z$ ALD process across a broad compositional range. We study films ranging from copper-free chromium oxide to chromium-free copper oxide by systematically changing the CuO_x:CrO_x cycle ratio via a super-cycle approach. The films are characterized in terms of their composition, structure and optoelectronic properties as well as their potential use as carrier-selective contacts in crystalline silicon solar cells.

2. Methods

$Cu_xCr_yO_z$ thin films were deposited using a commercial hot-wall flow-type F-120 ALD reactor (ASM Microchemistry Ltd, Finland). The Cu and Cr precursors were, respectively, in-house synthesized Cu(thd)$_2$ and Cr(acac)$_3$ (98 %), acquired from TCI chemicals. Ozone (O_3; Fisher model 502 generator) was used as the oxidant. The precursors were heated to 110 °C and 130 °C for Cu(thd)$_2$ and Cr(acac)$_3$, respectively. The deposition temperature was set at 250 °C for all samples, as the highest growth per cycle (GPC) was previously found at this value [52]. High purity N_2 (99.999 %) was used as both carrier and purging gas, with a reactor pressure between ~5–10 mbar. The deposition of these ternary oxide films was performed using a super-cycle approach of sequential deposition of CrO_x and CuO_x oxide layers. The sequence of the binary ALD cycles determines the final stoichiometry of the ternary compound. Based on our previous work, the pulse and purge times for both precursors were kept at 2 s and 3 s, respectively, throughout the study [52]. The films were deposited on single-side-polished (100) Si wafers with a native oxide layer. Low-resistivity (1–3 Ω cm) (100) p-type Si wafers, with a native oxide layer, were also used for contact resistivity measurements. A selection of films was annealed in a tube furnace under atmospheric pressure with an O_2 flow of ≈ 360 sccm, at 400–800 °C for 1 h.

Film thickness was characterized by X-ray reflectivity (XRR) using a PANanalytical model X'pert Pro diffractometer. Grazing-incidence X-ray diffraction (GIXRD) was used to extract the crystal structure information of the films using the PANalytical X'Pert PRO MRD system with Cu Kα radiation and an incident angle of 0.4°. A PHI5000 instrument was used to perform the x-ray photoelectron spectroscopy (XPS) measurements. An Al Kα (1486.6 eV) radiation source was used, operating at 10 kV and 24.6 W. The $Cu_xCr_{1-x}O_y$ thin films were analyzed by a combination of survey scans and core level scans for the peaks of interest, with step widths of 0.5 and 0.05 eV, respectively. The samples were analyzed as-introduced and after a succession of Ar^+-sputter steps (1x 1 min, 1 kV, 2x2). The XPS analysis of the core-level signals was performed using the CasaXPS software, with the deconvolution carried out by Shirley background processing and Gaussian functions [68].

Optical properties were extracted using an ex-situ J. A. Woollam M2000D spectroscopic ellipsometer. The data were fit using a B-spline model. Optical constants for either Cr_2O_3 or CuO were used as starting points for the fit. Work function and valence band energy were measured using a KP Technology Φ_4 ultrahigh-vacuum Kelvin probe system via contact potential difference and photoemission yield spectroscopy measurements, respectively. The work function uniformity was determined, in the same system, using a mapping mode. Transfer length measurements (TLM) were used to extract contact resistivity (ρ_c). The latter was performed by thermally evaporating 10 nm of palladium and 200 nm of silver metal on the films to form the TLM contact pads using a shadow mask. Current-voltage (*I-V*) measurements were performed using a Keithley 2425 SourceMeter at room temperature.

3. Results

The films were deposited using different cycle ratios of CuO_x/CrO_x to achieve a range of compositions from binary CrO_x to CuO_x. We varied the number of cycles (M, N) within each super cycle to achieve different compositions according to Fig. 1. The chosen ratios and cycle sequencing (M:N) were based on previous results reported for this process in combination with initial results for the binary CuO_x and CrO_x, with the goal to cover the entire compositional range. The growth per cycle values for the binary processes were 0.018 and 0.013 nm for CuO_x and CrO_x, respectively. According to the rule of mixtures (Equation (1) in supporting information), the resulting GPC for the ternary oxide should simply be given by the sum of the individual GPCs for the binary oxides weighted by the corresponding cycle ratio (Model 1). As such, we should, in principle, expect a linear change in GPC as we change the ratio of CuO_x and CrO_x cycles. However, we instead observed a highly non-linear dependence of GPC on the cycle ratio. Fig. 2(a) shows a sharp, almost 10 fold, increase in GPC (~0.1 nm/cycle) when increasing the CuO_x cycle ratio up to 0.25 (M:N = 1.3) and 0.5 (M:N = 1:1). The GPC subsequently drops to around 0.03 nm for higher CuO_x cycle ratios, though this is also significantly higher than for the binary CuO_x films.

Two mechanisms might explain this unexpected GPC behaviour. The first hypothesis is a potential precursor decomposition reaction during deposition, causing uncontrolled film growth. However, we found no

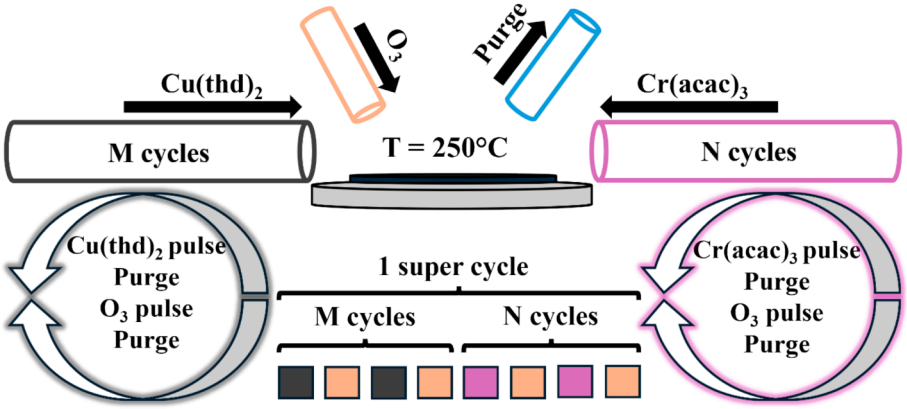

Fig. 1. Schematic figure representing the atomic layer deposition of $Cu_xCr_yO_z$ films. Super cycles were used to systematically change the M:N ratio of CuO_x and CrO_x cycles, respectively.

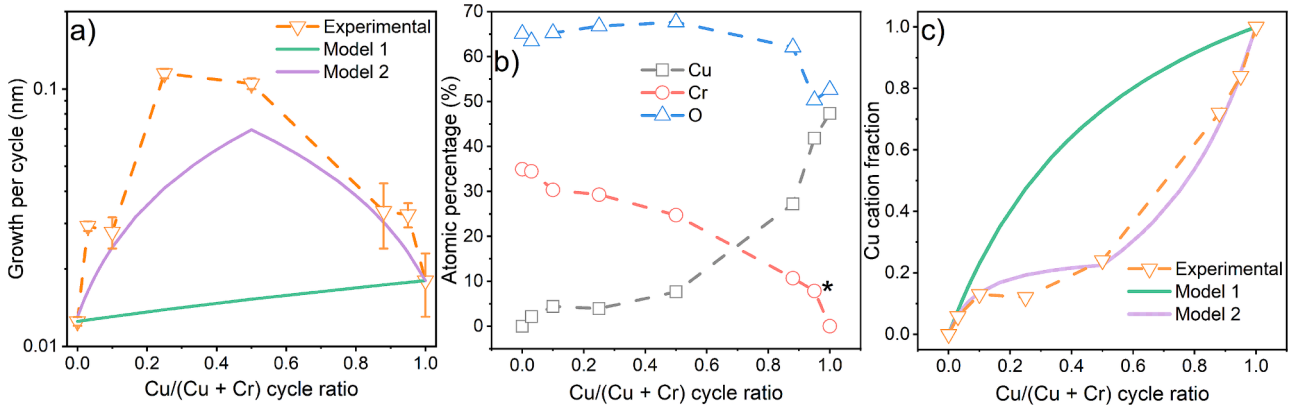

Fig. 2. (a) Growth per cycle (GPC) measured experimentally, and as predicted either by the rule of mixtures (Model 1), or with an enhanced growth (9×) for the first cycle of Cr following CuO_x (Model 2). (b) Compositional XPS analysis of the $Cu_xCr_yO_z$ films in terms of atomic percentage for Cu, Cr and O. (c) Experimental and predicted Cu cation fraction based on Model 1 and Model 2. All depositions were performed with ~700 cycles (M + N) in total. All data is presented as a function of the copper oxide cycle ratio. *The data point at a cycle ratio of 0.95 was calculated based on XPS measurements for the as-deposited sample (without sputtering).

signs of carbon incorporation originating from the precursor ligands in the films (see the XPS measurement in Figure S1 (d)), which would indicate precursor decomposition. Second, the gas-surface reactions in ALD are highly chemistry-dependent and thus the GPC values of binary materials can change drastically in the super cycle approach with the surface chemistry changing continuously. This might lead either to an enhanced or decreased surface nucleation and film growth [69]. To confirm this hypothesis and possibly deduce the reason for the increased GPC, we used XPS measurements to track the film composition, with the individual elemental atomic percentages shown in Fig. 2(b), and the copper cation fraction shown in Fig. 2(c). The compositions were determined from the XPS measurements performed on sputtered samples to remove potential surface contamination. The atomic percentages were derived by integrating the core level components for the elements of interest and applying the respective Scofield sensitivity factors. The complete XPS data set for the $Cu_xCr_yO_z$ films is displayed in Figure S1. We calculated the expected Cu cation fraction based on the rule of mixtures (Model 1) using Equations 2 and 3 (Supporting Information).

Fig. 2(c) shows the experimental and predicted copper cation fraction (C_{Cu}) as a function of copper cycle ratio. The data clearly show that the deposited films contain much less Cu than expected from the rule of mixtures (Model 1) which indicates that the sharp increase in GPC is due primarily to a higher incorporation of chromium oxide into the film. Therefore, we argue that this increase in GPC is related to an enhanced nucleation of the $Cr(acac)_3$ on the copper oxide surface. To support this hypothesis, we also modelled the expected GPC and C_{Cu} considering an enhanced deposition rate for the first cycle of CrO_x following a CuO_x cycle (Model 2). As shown in Fig. 2(c), this model is able to almost entirely reproduce the observed trend in the experimental cation fraction. An enhancement factor of 9 for the amount of chromium oxide deposited per cycle in the first CrO_x cycle was obtained from a fit of this model to the data. The model also provides significantly improved agreement with the measured GPC, as shown in Fig. 2(a). We note that a perfect fit in the case of GPC is not expected, since the calculation assumes that the CuO_x and CrO_x components maintain the densities of the respective binary compounds, which is unlikely to be the case given the formation of ternary phases. It is also worth noting that the film deposited with a Cu/(Cu + Cr) cycle ratio of 0.25 (M:N = 1:3) appears to be an outlier in terms of both GPC and cation fraction, which may point towards a more complex behaviour also for subsequent CrO_x cycles. Nevertheless, despite being a fairly simplistic approach to the potential complexity of the deposition behaviour across the full range of cycle ratios and film compositions, the excellent agreement of model and data confirms that the presence of CuO_x on the surface enhances the deposition of CrO_x. A possible speculative explanation is that the CuO_x surface somehow catalyses the dissociation and elimination of additional acac ligands from the adsorbed $Cr(acac)_3$ precursor, thereby reducing steric hindrance and increasing the fraction of surface sites available for $Cr(acac)_3$ adsorption. Table 1 summarizes the GPC, the actual and predicted Cu cation fraction, thickness, and the thin-film composition for different super cycles (M:N). All the following materials characterization was performed on films described in Table 1, unless otherwise stated.

Table 1
Summary of film properties for $Cu_xCr_yO_z$ compositions deposited using different CuO_x/CrO_x (M:N) cycle ratios.

M:N	Copper oxide cycle ratio	Thickness (nm)	GPC (nm)	Cu cation fraction	Cu cation fraction predicted (Model 1)	Cu cation fraction predicted (Model 2)	Cu at %	Cr at %	O at %
0:1	0	8.75	0.013	0	0	0	0	34.93	65.07
1:30	0.03	20.5	0.030	0.058	0.077	0.066	2.12	34.47	63.40
1:9	0.1	22.2	0.028	0.13	0.23	0.14	4.41	30.33	65.26
1:3	0.25	82.0	0.12	0.12	0.47	0.19	3.95	29.27	66.77
1:1	0.5	70.9	0.10	0.24	0.72	0.23	7.64	24.71	67.65
8:1	0.89	22.8	0.034	0.72	0.95	0.70	27.23	10.70	62.08
20:1	0.95	22.2	0.033	0.84	0.98	0.85	41.84	7.85	50.30
1:0	1	12.6	0.018	1	1	1	47.36	0	52.64

Additionally, throughout the paper, the data will be presented as a function of either Cu cation fraction or copper oxide cycle ratio.

Fig. 3 shows the GIXRD patterns for the different compositions in the as-deposited state, and after consecutive annealing at 400 and 800 °C for 1 h with a 360 sccm flow of O_2. For the Cu-rich films in the as-deposited state, we observe three peaks at 32.5°, 35.8°, and 38.8° corresponding to the (110), (002), and (111) planes of monoclinic CuO (JCPDS card no. 01–089-2531), indicating the presence of a polycrystalline film [70,71]. As the chromium fraction increases, we observe a drop in crystallinity, with the film becoming amorphous or weakly crystalline for a Cu cation fraction ≤24 %, with no apparent copper- or chromium-related peaks. We also observe a shift in the CuO peaks towards higher angles, which can be associated to the incorporation of Cr into the CuO matrix causing lattice distortion. Upon annealing at 400 °C (Fig. 3(b)), we observe the appearance of two new phases: Cr_2O_3 (Cu fraction 0–12 %) and $CuCr_2O_4$ (Cu fraction 24 %). The former presents peaks at 33.7° and 54.9°, which are the two most intense peaks for Cr_2O_3, corresponding to the [104] and [116] planes (JCPDS card no. 01-084-0313) [72,73]. Another report also obtained crystalline Cr_2O_3 by annealing at or above 400 °C [74]. The Cr_2O_3 peaks appeared clearly for all the Cr-rich films (Cr 87 % or more), except for the binary chromium oxide, where only weak diffraction peaks are apparent which can be attributed to the low film thickness (9 nm) and hence limited GIXRD sensitivity. Lastly, at a Cu cation fraction of 24 %, some peaks related to the spinel $CuCr_2O_4$ phase were detected. The peaks related to the $CuCr_2O_4$ phase at 30.9°, 35.3°, and 37.4° correspond to the [112], [211], and [202] planes (JCPDS card no. 05-0657) [40]. The $CuCr_2O_4$ phase was also observed in our previous work when using a cycle ratio M:N of 1:4 and performing a rapid thermal annealing at 700 °C in O_2 [40]. Here, we observe the phase for a 1:1 cycle ratio film, which may indicate an influence of different annealing conditions on the phase formation. When increasing the annealing temperature to 800 °C (Fig. 3(c)), other peaks related to the $CuCr_2O_4$ phase appear at 29.5°, 42.4°, 56.2°, 58.1°, 61.46°, and 64.8°, which correspond to the [200], [220], [321], [303], [400] and [411] planes, [40] respectively. Additionally, the peaks detected already at 400 °C become more intense, indicating improved $CuCr_2O_4$ crystallinity. At 800 °C, the CuO peaks for the two most Cu-rich films are significantly reduced in intensity, which may be associated with the formation of a porous film as previously reported at 750 °C [75]. At the same time, the CuO peaks for all the Cu-rich films (≥ 72 % Cu cation fraction) become sharper, indicating higher crystallinity.

Notably, apart from changes in the degree of crystallinity, no major phase transformation is observed to take place. The $CuCrO_2$ delafossite phase formation is not observed, even at 800 °C, in contrast to our previous report [52]. However, a direct comparison with the present work is not possible, due to the different annealing conditions used. Apart from the annealing conditions, a major factor explaining the lack of $CuCrO_2$ phase formation is the Cu/(Cu + Cr) cation fraction. According to the phase diagram and Gibbs free energy of formation for the $Cu_xCr_yO_z$ system, it is not possible to form $CuCrO_2$ at ≈ 400 °C considering the compositions of the films in this work [25]. According to the phase diagram, for pO_2 of 0.21 atm, $CuCr_2O_4$ is always formed with either CuO (for Cu cation fraction > ≈ 0.33) or Cr_2O_3 (for Cu cation fraction < ≈ 0.33). On the other hand, at a higher annealing temperature (≈782 °C), the formation of some $CuCrO_2$ has been reported for a Cu cation fraction >0.5 [25]. However, this was not observed in this work, which may result from a different pO_2 and/or insufficient annealing time. We should note that, as no XPS measurements were performed in our previous work, the overall composition of the as-deposited and annealed films from that work is strictly unknown. Therefore, despite the observation of a delafossite phase, we cannot exclude the possibility that those films were similarly Cr-rich.

We also investigated the effects of the cycle ratio, and annealing, on the optical properties of the $Cu_xCr_yO_z$ thin films. For these measurements, the annealing was performed at 400–800 °C with 100 °C intervals. Fig. 4 shows the absorption coefficient for different Cu cation fractions before and after annealing at different temperatures. We observe a clear difference between films with Cu <24 at% and the ones with higher Cu content (> 72 at%). At the lower Cu fractions, the film presents a lower absorption in the 300–450 nm range due to the absence of the more absorbing CuO phase.

As the samples were progressively annealed, the distinction between the Cu- and Cr-rich films became more evident, with the former increasing their absorption in the visible range. The reduction in the intensity of the CuO GIXRD peaks at 400 °C and 800 °C for the Cu 100 at % and 84 at% films could explain this higher absorption. Despite a distinct copper metal phase not being directly observed in the GIXRD measurements, some Cu reduction may have occurred. The formation of Cu metal would be expected to lead to a higher absorption in the visible range. In fact, some Cu-rich samples were unmeasurable via ellipsometry after annealing at high temperatures, in the sense that the raw measurement data could not be adequately described using a layer with homogenous optical properties, and their optical properties are consequently not reported at those temperatures. This may point to the segregation of metallic copper grains, even though these are not observed by XRD; or the diffusion of Cu into silicon, forming metallic Cu_3Si, which may be invisible in GIXRD and is usually detected in Bragg–Brentano configuration. At 800 °C, the Cu 24 at% film, which exhibited a pure $CuCr_2O_4$ spinel phase in GIXRD, displayed a high absorption in the visible range, [76] and it was not possible to identify the onset of band-to-band absorption. A previous report has linked the $CuCr_2O_4$ spinel phase to a metallic-like behaviour, [43] but we cannot confirm this based on the ellipsometry data alone.

From the absorption coefficient measurements, we used the Tauc plot analysis (Figure S2 and S3) to extract the band gap (E_g), when possible. We considered a direct allowed (n = 1/2) transition for the samples with Cu content less than 24 % (i.e. 0, 6, 13, 12, and 24 %), and an indirect allowed (n = 2) transition for the samples with Cu 72, 84 and 100 at%. These choices were made based on band gap transition of CuO and Cr_2O_3, which are indirect allowed and direct allowed, respectively. Fig. 5(a) shows the extracted band gap for the different Cu cation fractions and annealing temperatures. The addition of Cr into the film leads to a wider band gap for films with a Cr-rich composition (direct allowed transition) whereas films with a Cu-rich composition (indirect allowed transition) had their band gap decreased with the incorporation of chromium. Annealing at 400 °C increased the apparent band gap at all

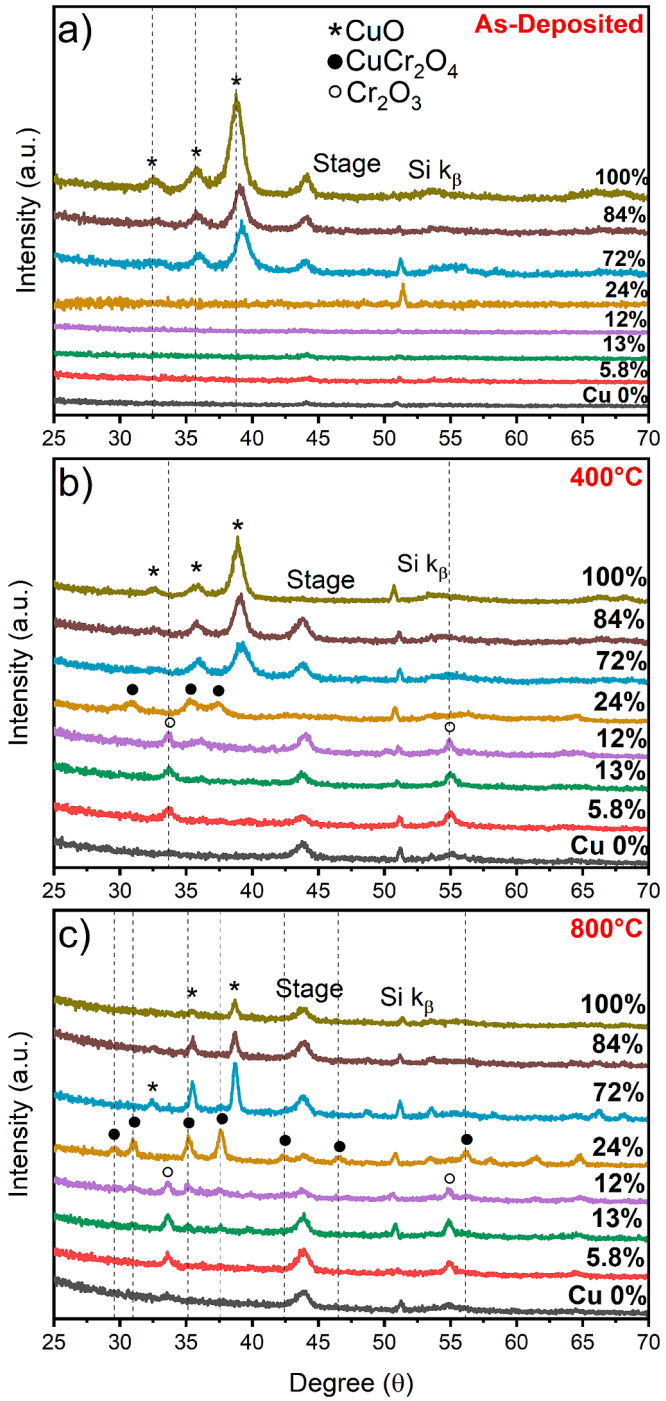

Fig. 3. GIXRD of different $Cu_xCr_yO_z$ compositions (a) in the as-deposited state and annealed at (b) 400 °C and (c) 800 °C for 30 min. The at% indicates the Cu cation fraction present in the films as obtained from XPS.

compositions. Upon further annealing at 500–700 °C, the band gap first drops for the Cr-rich films but then remains relatively stable and higher than the as-deposited value. For the Cu-rich films, it became increasingly difficult to extract reliable band gap values upon annealing at 500 °C or higher, as was also the case for some of the Cr-rich films at 800 °C, due to apparent increase in surface roughness making the use of ellipsometry unreliable.

Fig. 5(b) displays the refractive index extracted for the different compositions before and after annealing. We observe a clear trend of decrease in refractive index with increasing annealing temperature for Cr_2O_3, which is similar to a previous report.[74] CuO, on the other hand, showed an initial increase in refractive index at 400 °C before dropping at higher temperatures. The drop of refractive index to values <1 after annealing for the Cu-rich films is another indicator of Cu_3Si formation as it presents a metallic behaviour with reported refractive index <1 [77], potentially together with the presence of voids in the films, consistent with the absorption coefficient data and the drop in intensity of the CuO peaks in the GIXRD spectra. The complete refractive index and extinction coefficient spectra for the different copper oxide cycle ratios are reported in Figures S4 and S5, respectively.

The work function (WF) is an important material property for the development and application of semiconductor materials, especially for energy-related applications. Fig. 6(a) shows the work function of the as-deposited $Cu_xCr_yO_z$ compounds as a function of the copper oxide cycle ratio. Cr_2O_3 presented a WF of 4.75 eV, which falls within the expected range reported in the literature [78]. As we incorporate copper into the film, the WF increases, reaching values of ≈ 5.10 eV for Cu cycle ratios of 0.1 and 0.25 (Cu 13 and 12 at%). Similar behaviour has been previously reported for a Cu-doped CrO_x film [79]. For higher Cu concentrations, the work function drops and remains relatively stable at ≈ 4.85 eV for the remaining compositional range up to CuO. Upon annealing at 400 °C, work function greatly increases, as shown in Fig. 6(b), with values above 6 eV for several of the Cr-rich films. These values are comparable to those obtained for high-work-function materials such as MoO_3, V_2O_5, and WO_3, which are important hole-selective contacts for silicon solar cells [56]. After further annealing at 500 and 600 °C, the work function drops, though it remains above the as-deposited state. Low work function values (≈ 4.5 eV) are found for the Cu-rich films annealed at 700 and 800 °C. As, to the best of our knowledge, there are no previous reports on the work function of $CuCr_2O_4$, it is important to highlight the value of 5.0 ± 0.2 eV obtained, which corresponds to a 0.5 copper oxide cycle ratio (Cu 24 at%) after annealing at 700–800 °C. The work function uniformity was evaluated by mapping a ≈ 0.5 cm^2 area using the Kelvin probe system; Figure S6 (colour maps) shows the high uniformity for the as-deposited films. The mapping also confirmed that the films remained uniform upon annealing (indicated by the error bars in Fig. 6). The only exception was the $CuCr_2O_4$ sample, formed on annealing at 800 °C using a 0.5 copper oxide cycle ratio, which presented significantly higher non-uniformity as indicated by the associated error bars in Fig. 6.

Photoemission yield spectroscopy measurements were performed for the as-deposited $Cu_xCr_yO_z$ samples as shown in Figure S7. From the resulting curves, we extracted the valence band maxima by fitting the linear portion of the data. With the work function, valence band maximum (VBM), and band gap, we calculated the conduction band minimum (CBM) and plotted the energy band diagram of the as-deposited $Cu_xCr_yO_z$ thin films. Fig. 7 shows the diagrams for each Cu cation fraction obtained in the ALD. To function as carrier-selective contacts in solar cells, these films need to present a small valence (conduction) band offset with the absorber to allow the passage of holes (electrons) while maintaining a high conduction (valence) band offset to block electrons (holes). Additionally, a high (low) work function also benefits the conduction of holes (electrons) by providing an upward (downward) band bending at the absorber interface leading to a higher hole (electron) concentration at the surface. Given the CBM and VBM of crystalline silicon are 4.05 and 5.17 eV, respectively, films with higher Cu (>72 %) present both very small CBM and VBM offsets, and thus are not good candidates to be employed as carrier-selective contacts. On the other hand, films with lower Cu content (<24 at%) present a high conduction band offset with silicon. More importantly, samples with 5.8–13 % of Cu seem to be particularly suitable candidates as hole-selective contacts in c-Si solar cells as they also present a relatively small valence band offset of 0.17–0.21 eV and relatively high work functions above 5 eV.

Given the high potential of some of these films as hole-selective contacts for c-Si, we proceeded to prepare contact resistivity (ρ_c) test samples on low-resistivity p-type Si wafers. Determination of the value

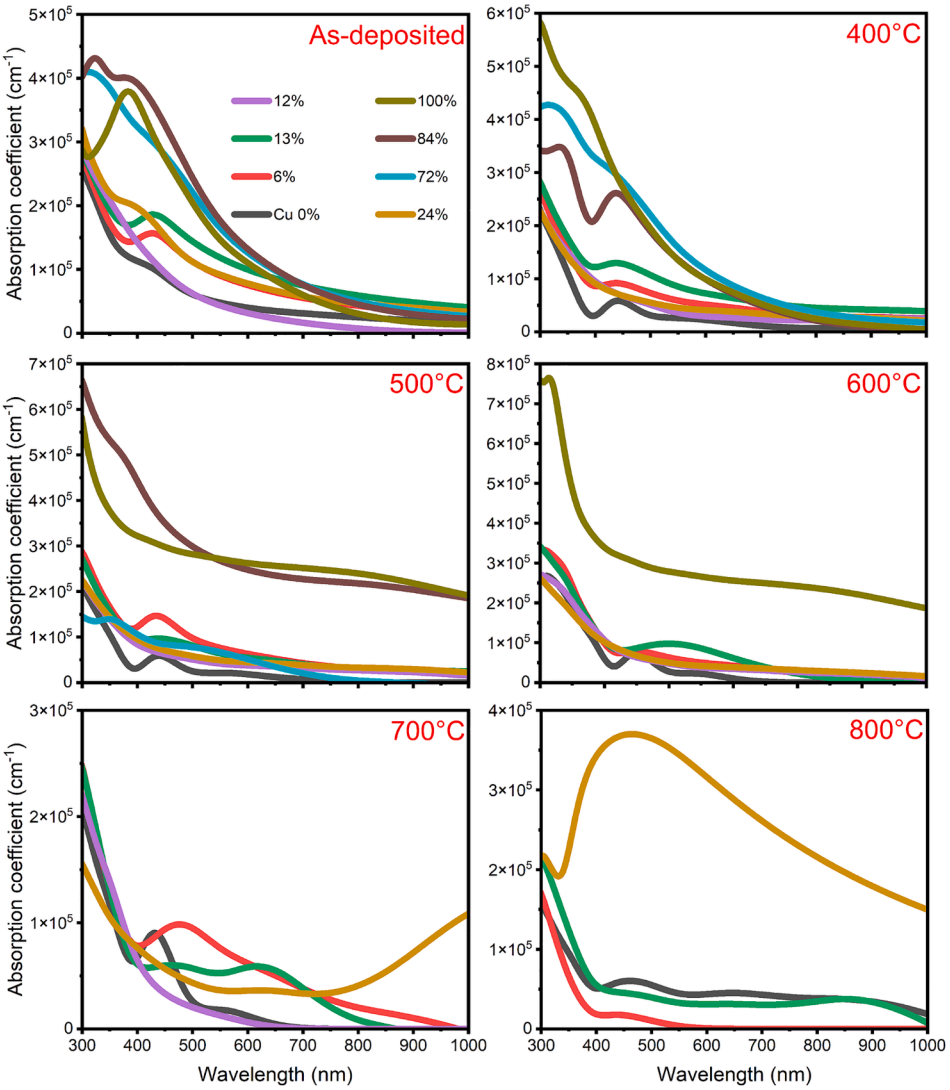

Fig. 4. Absorption coefficient of $Cu_xCr_yO_z$ thin films as a function of the Cu cation fraction and annealing temperature.

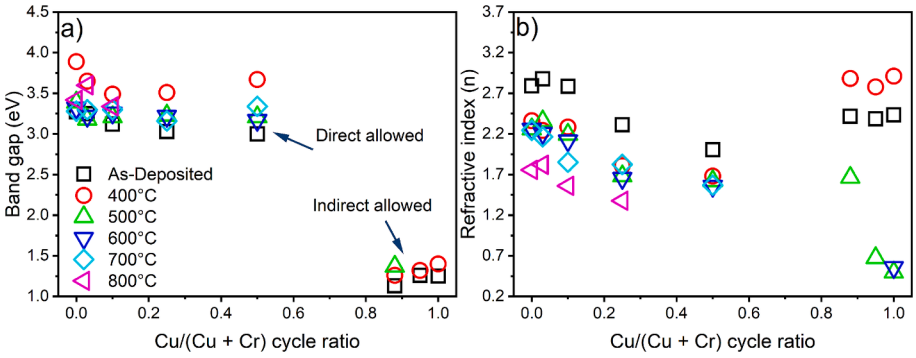

Fig. 5. (a) Band gap and (b) refractive index of $Cu_xCr_yO_z$ thin films deposited at different cycle ratios and annealed at various temperatures.

of ρ_c is particularly important to establish whether these ternary compounds have potential to work as hole-selective contacts in c-Si solar cell devices. Based on previous reports, [80,81] a film thickness of 4 nm was selected for the ρ_c measurements. The required cycle count was estimated from the measured GPC of the thicker films and the resulting thickness was confirmed by ellipsometry. Both as-deposited and annealed (at 400 °C) films were investigated, the latter because they presented the highest WFs. Transfer length method (TLM) contact patterns were formed using stacks of evaporated palladium and silver, as shown schematically in Fig. 8(a). Fig. 8(b) shows the extracted ρ_c as a function of the copper oxide cycle ratio. We observe a considerable drop in ρ_c as we begin to add copper to the Cr_2O_3 films. When comparing to Fig. 6(a) and Fig. 7, the drop in ρ_c for these Cr-rich films correlates closely with the increase in work function and reduction in the VBM offset. As well-reported in the literature, the contact performance of hole-selective materials benefits from high work function values (> 5

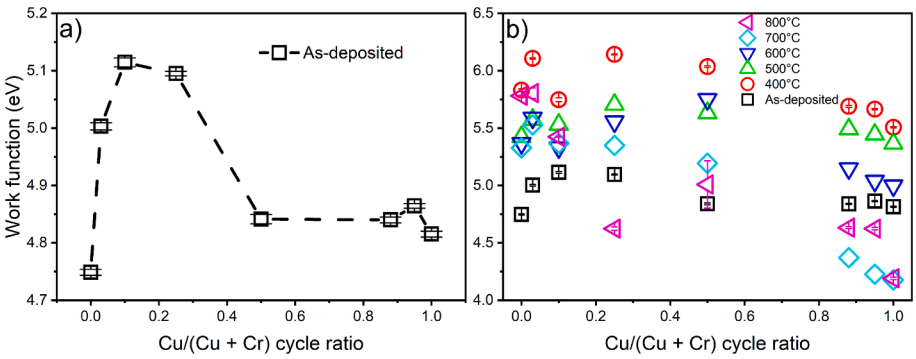

Fig. 6. Work function of the $Cu_xCr_yO_z$ thin films deposited at different cycle ratios for both (a) as-deposited and (b) successively annealed at indicated temperatures. Error bars indicate standard deviation across a ≈ 0.5 cm^2 area.

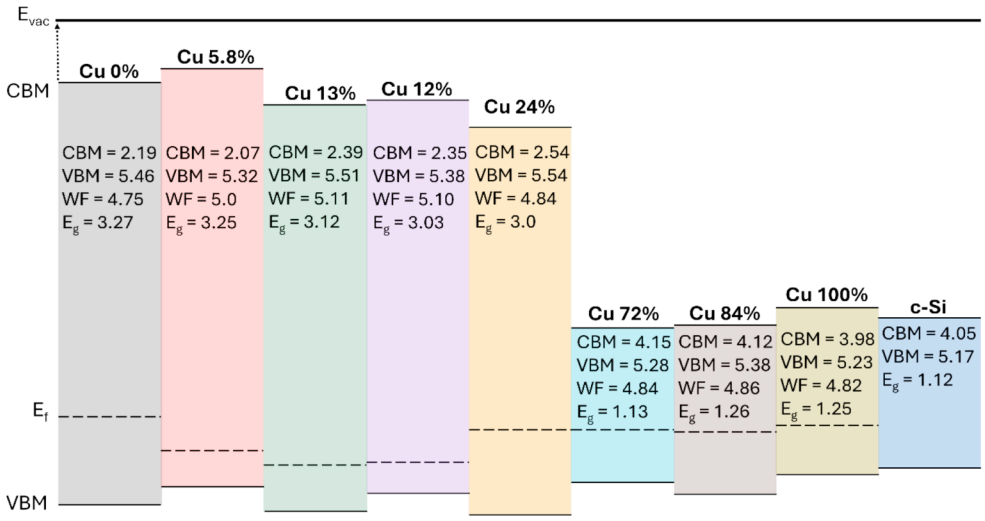

Fig. 7. Energy band diagram of $Cu_xCr_yO_z$ films containing different Cu cation fractions. CBM, E_f, VBM, and E_g represent the conduction band minimum, fermi level, valence band maximum, and band gap, respectively.

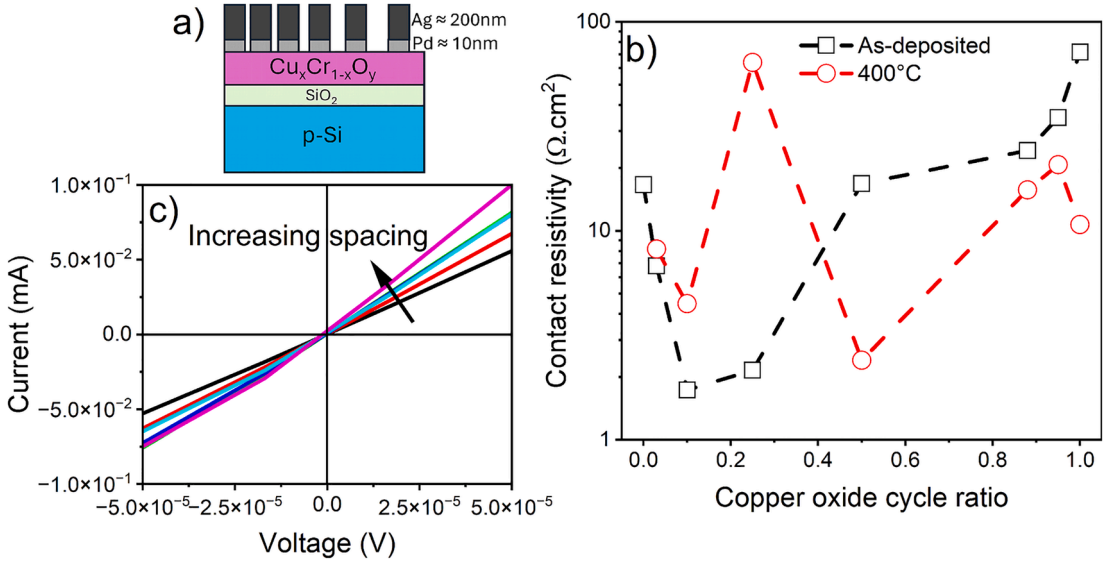

Fig. 8. (a) Schematic diagram of the TLM samples employed for the contact resistivity measurements. (b) Extracted contact resistivity as a function of the copper oxide cycle ratio for ~4 nm thick films both as-deposited and annealed at 400 °C. (c) IV curves for the sample with the lowest contact resistivity (CuO_x cycle ratio = 0.1; 13 % Cu).

eV) [55,82]. This behaviour is well-represented here as the sample with 13 % Cu cation fraction (Cu cycle ratio of 0.1) demonstrates both the highest work function (5.11 eV) and lowest contact resistivity (1.72 Ω cm^2) among the as-deposited samples.

The IV curves measured for the lowest contact resistivity sample (CuO_x cycle ratio = 0.1 and 13 % Cu cation fraction) are shown in Fig. 8 (c), indicating a near-ohmic behaviour in the measured range. We would expect a further decrease in ρ_c upon annealing at 400 °C as the work function increases. However, as seen from Figs. 6 and 8(b), the increase in WF was not found to correlate to a considerable drop in contact resistivity. In fact, for Cr-rich films, the contact resistivity after annealing was higher than in the as-deposited case. Despite a higher work function at 400 °C, other effects might hinder the contact resistivity, such as chemical reduction of Cu/Cr at the silicon interface or effusion of passivating hydrogen, increasing the density of interface states and possibly leading to Fermi level pinning and therefore higher contact resistivity [83]. In this context, it should be noted that these samples were fabricated on silicon wafers with a native silicon oxide present and without the use of a standard chemical cleaning step (such as an RCA clean), and therefore the Si interface of even the as-deposited samples is possibly not of high electronic quality, which may have resulted in higher values of ρ_c than would have been obtained on clean surfaces. Therefore, despite showing a similar trend, the absolute value is higher than that observed for spin-coated CrO_x:Cu films (95 mΩ cm^2) [54]. At 500 °C, the contact resistance greatly increased, and we were unable to confidently extract its value. Overall, despite the high work functions and transparency obtained for some compositions, the contact resistivity remains relatively high for contact applications in c-Si devices such as solar cells. Further optimization of process parameters such as deposition and annealing temperature together with the use of interlayers may contribute to further decrease the contact resistivity and improve the performance of $Cu_xCr_yO_z$ ternary oxides as hole-selective contacts to c-Si.

4. Conclusion

$Cu_xCr_yO_z$ ternary compound films with varying composition were produced by ALD at 250 °C using a wide range of CrO_x:CuO_x cycle ratios. Films with intermediate compositions presented enhanced GPC, reaching ~7–10 times higher (0.12 nm/cycle) compared to the binary oxide depositions. The increase in GPC was determined to be caused by an enhanced nucleation of $Cr(acac)_3$ on the CuO_x surface: a growth model assuming 9 times higher GPC for the first CrO_x cycle after CuO_x cycle was found to reproduce the experimental GPC and compositional trends appreciably well. The as-deposited films containing high amounts of copper were crystallized in the CuO phase. Upon annealing at 400 and 800 °C, diffraction peaks related to crystalline Cr_2O_3 and $CuCr_2O_4$ appeared for films with higher concentrations of chromium. Optical measurements indicated higher absorption for Cu-rich films, which was also represented by a decrease in band gap as the CuO_x cycle ratio increased. Annealing at 400 °C resulted in an initial rise in band gap, followed by a slight decrease across all compositions with continued annealing at higher temperatures. Work function values peaked for Cr-rich films, reaching ~5.1 eV for a 13 % Cu cation fraction. Upon annealing at 400 °C, Cr-rich compositions reached work functions above 6 eV before dropping to ≈ 5.5 eV at higher annealing temperatures (500–800 °C). Additionally, it is important to highlight the work function of ~5 eV obtained for the films containing the spinel phase $CuCr_2O_4$, which has not previously been reported. The as-deposited thin films and those annealed at 400 °C were tested as potential hole-selective contacts to c-Si. The film containing a Cu cation fraction of 13 % ($Cu_{0.05}Cr_{0.30}O_{0.65}$) reached the lowest ρ_c of 1.72 Ω cm^2 in the as-deposited state, showing its potential to work as a transparent hole-selective contact for c-Si devices such as solar cells. As demonstrated here, ALD provides an efficient route for the growth of ternary Cu-based films with precise control over different stoichiometries. We hope this work may serve as a basis for the future development of Cu-based ternary compounds for solar cells and other optoelectronic applications.

CRediT authorship contribution statement

Gabriel Bartholazzi: Writing – original draft, Methodology, Investigation, Formal analysis, Data curation, Conceptualization. **Topias Jussila:** Writing – review & editing, Methodology. **Jorit Obenlüneschloß:** Writing – review & editing, Data curation. **Ville Vähänissi:** Writing – review & editing, Supervision, Resources. **Anjana Devi:** Writing – review & editing, Resources. **Hele Savin:** Writing – review & editing, Supervision, Resources. **Maarit Karppinen:** Writing – review & editing, Supervision, Resources. **Daniel H. Macdonald:** Writing – review & editing, Supervision, Resources, Project administration, Funding acquisition. **Lachlan E. Black:** Writing – review & editing, Validation, Supervision, Resources, Project administration, Funding acquisition, Formal analysis.

Declaration of competing interest

The authors declare that they have no known competing financial interests or personal relationships that could have appeared to influence the work reported in this paper.

Acknowledgements

This work has been supported by the Australian Renewable Energy Agency (ARENA) through the Australian Centre for Advanced Photovoltaics (ACAP). Funding was received from the European Union (ERC AdG, UniEnMLD, No. 101097815). Views and opinions expressed are however those of the authors only and do not necessarily reflect those of the European Union or the European Research Council. Neither the European Union nor the granting authority can be held responsible for them. The authors acknowledge the provision of facilities and technical support by Micronova Nanofabrication Centre in Espoo, Finland within the OtaNano research infrastructure at Aalto University. The work is part of the Research Council of Finland Flagship Programme, Photonics Research and Innovation (PREIN), decision number 346529.

Appendix A. Supplementary material

Supplementary data to this article can be found online at https://doi.org/10.1016/j.apsusc.2024.161793.

Data availability

Data will be made available on request.

References

[1] B.G. Lewis, D.C. Paine, Applications and processing of transparent conducting oxides, MRS Bull. 25 (2000) 22–27.
[2] D.S. Ginley, C. Bright, Transparent conducting oxides, MRS Bull 25 (2000) 15–18.
[3] T.S. Tripathi, M. Karppinen, Atomic layer deposition of p-type semiconducting thin films: a review, Adv. Mater. Interf. 4 (2017).
[4] H. Lin, et al., Silicon heterojunction solar cells with up to 26.81% efficiency achieved by electrically optimized nanocrystalline-silicon hole contact layers, Nat. Energy 8 (2023) 789–799.
[5] K.H.L. Zhang, K. Xi, M.G. Blamire, R.G. Egdell, P -type transparent conducting oxides, J. Phys. Condens. Matter 28 (2016) 383002.
[6] Z. Wang, P.K. Nayak, J.A. Caraveo-Frescas, H.N. Alshareef, Recent developments in p-type oxide semiconductor materials and devices, Adv. Mater. 28 (2016) 3831–3892.
[7] M.-S. Miao, S. Yarbro, P.T. Barton, R. Seshadri, Electron affinities and ionization energies of Cu and Ag delafossite compounds: A hybrid functional study, Phys. Rev. B 89 (2014) 045306.
[8] A.N. Banerjee, K.K. Chattopadhyay, Recent developments in the emerging field of crystalline p-type transparent conducting oxide thin films, Prog. Cryst. Growth Charact. Mater. 50 (2005) 52–105.
[9] N. Zhang, J. Sun, H. Gong, Transparent p-type semiconductors: copper-based oxides and oxychalcogenides, Coatings 9 (2019) 137.

[10] R.D. Shannon, D.B. Rogers, C.T. Prewitt, J.L. Gillson, Chemistry of noble metal oxides. III. electrical transport properties and crystal chemistry of ABO_2 compounds with the delafossite structure, Inorg. Chem. 10 (1971) 723–727.

[11] R.D. Shannon, D.B. Rogers, C.T. Prewitt, Chemistry of noble metal oxides. I. syntheses and properties of ABO_2 delafossite compounds, Inorg. Chem. 10 (1971) 713–718.

[12] R.D. Shannon, C.T. Prewitt, D.B. Rogers, Chemistry of noble metal oxides. II. Crystal structures of platinum cobalt dioxide, palladium cobalt dioxide, coppper iron dioxide, and silver iron dioxide, Inorg. Chem. 10 (1971) 719–723.

[13] H. Kawazoe, et al., P-type electrical conduction in transparent thin films of $CuAlO_2$, Nature 389 (1997) 939–942.

[14] H. Yanagi, et al., Electronic structure and optoelectronic properties of transparent p -type conducting $CuAlO_2$, J. Appl. Phys. 88 (2000) 4159–4163.

[15] M.M. Moharam, M.M. Rashad, E.M. Elsayed, R.M. Abou-Shahba, A facile novel synthesis of delafossite $CuFeO_2$ powders, J. Mater. Sci. Mater. Electron. 25 (2014) 1798–1803.

[16] H. Mohamed, et al., Synthesis of conducting single-phase $CuFeO_2$ thin films by spray pyrolysis technique, Mater. Sci. Semicond. Process 107 (2020) 104831.

[17] C. Ruttanapun, Optical and electronic properties of delafossite $CuBO_2$ p -type transparent conducting oxide, J. Appl. Phys. 114 (2013) 113108.

[18] H. Yanagi, T. Hase, S. Ibuki, K. Ueda, H. Hosono, Bipolarity in electrical conduction of transparent oxide semiconductor $CuInO_2$ with delafossite structure, Appl. Phys. Lett. 78 (2001) 1583–1585.

[19] K. Ueda, et al., Epitaxial growth of transparent p-type conducting $CuGaO_2$ thin films on sapphire (001) substrates by pulsed laser deposition, J. Appl. Phys. 89 (2001) 1790–1793.

[20] H. Zhang, H. Wang, W. Chen, A.K.Y. Jen, $CuGaO_2$: A promising inorganic hole-transporting material for highly efficient and stable perovskite solar cells, Adv. Mater. 29 (2017).

[21] R.S. Yu, D.H. Hu, Formation and characterization of p-type semiconductor $CuCrO_2$ thin films prepared by a sol-gel method, Ceram. Int. 41 (2015) 9383–9391.

[22] T.S. Tripathi, M. Karppinen, Enhanced p-type transparent semiconducting characteristics for ALD-grown mg-substituted $CuCrO_2$ thin films, Adv. Electron. Mater. 3 (2017) 1–7.

[23] S. Götzendörfer, C. Polenzky, S. Ulrich, P. Löbmann, Preparation of $CuAlO_2$ and $CuCrO_2$ thin films by sol-gel processing, Thin Solid Films 518 (2009) 1153–1156.

[24] M. Moreira, J. Afonso, J. Crepelliere, D. Lenoble, P. Lunca-Popa, A review on the p-type transparent Cu–Cr–O delafossite materials, J. Mater. Sci. 57 (2022) 3114–3142.

[25] J. Schorne-Pinto, P. Chartrand, A. Barnabé, L. Cassayre, Thermodynamic and structural properties of $CuCrO_2$ and $CuCr_2O_4$: experimental investigation and phase equilibria modeling of the Cu–Cr–O system, J. Phys. Chem. C 125 (2021) 15069–15084.

[26] J. Kim, et al., Highly conductive and visibly transparent p-type $CuCrO_2$ films by ultrasonic spray pyrolysis, ACS Appl. Mater. Interf. 14 (2022) 11768–11778.

[27] H. Zhang, et al., Low-temperature solution-processed $CuCrO_2$ hole-transporting layer for efficient and photostable perovskite solar cells, Adv. Energy Mater. 8 (2018).

[28] M. Huang, et al., O, N co-doped $CuCrO_2$ as efficient hole transport layer for high-performance ultraviolet photodetectors, J. Alloys Compd. 971 (2024) 172743.

[29] R.-S. Yu, C.-M. Wu, Characteristics of p-type transparent conductive $CuCrO_2$ thin films, Appl. Surf. Sci. 282 (2013) 92–97.

[30] B. Zhang, et al., Mg doped $CuCrO_2$ as efficient hole transport layers for organic and perovskite solar cells, Nanomaterials 9 (2019) 1311.

[31] T.S. Tripathi, M. Karppinen, Structural optical and electrical transport properties of ALD-fabricated CuCrO2 films, Physics Procedia 75 (2015) 488–494.

[32] D.O. Scanlon, G.W. Watson, Understanding the p-type defect chemistry of $CuCrO_2$, J. Mater. Chem. 21 (2011) 3655.

[33] S.S. Acharyya, S. Ghosh, S. Adak, T. Sasaki, R. Bal, Facile synthesis of $CuCr_2O_4$ spinel nanoparticles: a recyclable heterogeneous catalyst for the one pot hydroxylation of benzene, Catal. Sci. Technol. 4 (2014) 4232–4241.

[34] S.S. Acharyya, S. Ghosh, R. Bal, Catalytic oxidation of aniline to azoxybenzene over $CuCr_2O_4$ spinel nanoparticle catalyst, ACS Sustain. Chem. Eng. 2 (2014) 584–589.

[35] P. Liu, E.J.M. Hensen, Highly efficient and robust Au/$MgCuCr_2O_4$ catalyst for gas-phase oxidation of ethanol to acetaldehyde, J. Am. Chem. Soc. 135 (2013) 14032–14035.

[36] S. Boumaza, R. Bouarab, M. Trari, A. Bouguelia, Hydrogen photo-evolution over the spinel $CuCr_2O_4$, Energy Convers. Manag. 50 (2009) 62–68.

[37] R.M. Mohamed, M.W. Kadi, Generation of hydrogen gas using $CuCr_2O_4$-g-C_3N_4 nanocomposites under illumination by visible light, ACS Omega 6 (2021) 4485–4494.

[38] Y. Youn, et al., Effects of metal dopings on $CuCr_2O_4$ pigment for use in concentrated solar power solar selective coatings, ACS Appl. Energy Mater. 2 (2019) 882–888.

[39] R. Bajaj, M. Sharma, D. Bahadur, Visible light-driven novel nanocomposite ($BiVO_4$/$CuCr_2O_4$) for efficient degradation of organic dye, Dalton Trans. 42 (2013) 6736.

[40] T.S. Tripathi, C.S. Yadav, M. Karppinen, Transparent ferrimagnetic semiconducting $CuCr_2O_4$ thin films by atomic layer deposition, APL Mater. 4 (2016).

[41] K. Y, et al., Structural transformation and magnetic properties of Fe-substituted nano $CuCr_2O_4$ spinel structure, Ceram. Int. 50 (2024) 4987–4993.

[42] P. Sankudevan, et al., Enhancement of luminescence mechanisms in structural, morphological, and catalytic properties of undoped $CuCr_2O_4$ and Mn-Doped $CuCr_2O_4$, J. Clust. Sci. 34 (2023) 1527–1534.

[43] R. Bencheikh, K. Belakroum, Theoretical study of the spinel structure of $CuCr_2O_4$ in the tetragonal phase using density functional theory, J. Nano- Electr. Phys. 14 (2022) 05030-1–05030-7.

[44] S. Sundaresh, A.H. Bharath, K.B. Sundaram, Effect of annealing temperature on radio frequency sputtered p-type delafossite copper chromium oxide ($CuCrO_2$) thin films and investigation of diode characteristics forming transparent pn-heterojunction, Coatings 13 (2023).

[45] D.C. Tsai, E.C. Chen, Y.L. Huang, F.S. Shieu, Z.C. Chang, Annealing effect on the structural and optoelectronic properties of Cu-Cr-O thin films deposited by reactive magnetron sputtering using a single CuCr target, Mater. Sci.- Poland 41 (2023) 191–201.

[46] H.-Y. Chen, K.-P. Chang, Influence of post-annealing conditions on the formation of delafossite-$CuCrO_2$ Films, ECS J. Solid State Sci. Technol. 2 (2013) P76–P80.

[47] P.W. Sadik, M. Ivill, V. Craciun, D.P. Norton, Electrical transport and structural study of $CuCr_{1-x}Mg_xO_2$ delafossite thin films grown by pulsed laser deposition, Thin Solid Films 517 (2009) 3211–3215.

[48] D. Li, et al., Physical properties of $CuCrO_2$ films prepared by pulsed laser deposition, Vacuum 84 (2010) 851–856.

[49] L. Bottiglieri, A. Nourdine, J. Resende, J.L. Deschanvres, C. Jiménez, Optimized stoichiometry for $CuCrO_2$ thin films as hole transparent layer in PBDD4T-2F: PC70BM organic solar cells, Nanomaterials 11 (2021) 1–15.

[50] P. Lunca-Popa, et al., Tuning the electrical properties of the p-type transparent conducting oxide Cu1−xCr1+xO2 by controlled annealing, Sci. Rep. 8 (2018) 7216.

[51] P. Lunca Popa, J. Crèpellière, R. Leturcq, D. Lenoble, Electrical and optical properties of Cu–Cr–O thin films fabricated by chemical vapour deposition, Thin Solid Films 612 (2016) 194–201.

[52] T.S. Tripathi, J.P. Niemelä, M. Karppinen, Atomic layer deposition of transparent semiconducting oxide $CuCrO_2$ thin films, J. Mater. Chem. C Mater. 3 (2015) 8364–8371.

[53] L. Bottiglieri, et al., Out of stoichiometry $CuCrO_2$ films as a promising p-type TCO for transparent electronics, Mater. Adv. 2 (2021) 4721–4732.

[54] Z. Xu, et al., Solution-processed copper-doped chromium oxide with tunable oxygen vacancy for crystalline silicon solar cells hole-selective contacts, Sol. RRL 5 (2021).

[55] J. Melskens, et al., Passivating contacts for crystalline silicon solar cells: from concepts and materials to prospects, IEEE J. Photovolt. 8 (2018) 373–388.

[56] Y. Wang, S.T. Zhang, L. Li, X. Yang, L. Lu, D. Li, Dopant-free passivating contacts for crystalline silicon solar cells: Progress and prospects, EcoMat 5 (2) (2023) e12292, https://doi.org/10.1002/eom2.12292.

[57] M. Sun, et al., Interface modification with $CuCrO_2$ nanocrystals for highly efficient and stable planar perovskite solar cells, ACS Appl. Mater. Interf. 14 (2022) 13352–13360.

[58] X. Zhang, Y. Wan, J. Bullock, T. Allen, A. Cuevas, Low resistance Ohmic contact to p-type crystalline silicon via nitrogen-doped copper oxide films, Appl. Phys. Lett. 109 (2016).

[59] J. Wang, Y.-J. Lee, J.W.P. Hsu, Sub-10 nm copper chromium oxide nanocrystals as a solution processed p-type hole transport layer for organic photovoltaics, J. Mater. Chem. C Mater. 4 (2016) 3607–3613.

[60] W.A. Dunlap-Shohl, et al., Room-temperature fabrication of a delafossite $CuCrO_2$ hole transport layer for perovskite solar cells, J. Mater. Chem. A Mater. 6 (2018) 469–477.

[61] L. Bottiglieri, A. Nourdine, J. Resende, J.-L. Deschanvres, C. Jiménez, Optimized stoichiometry for $CuCrO_2$ thin films as hole transparent layer in PBDD4T-2F: PC70BM organic solar cells, Nanomaterials 11 (2021) 2109.

[62] W. Lin, et al., Novel hole selective CrOx contact for dopant-free back contact silicon solar cells, Mater. Res. Bull. 103 (2018) 77–82.

[63] W. Lin, et al., Chromium trioxide hole-selective heterocontacts for silicon solar cells, ACS Appl. Mater. Interf. 10 (2018) 13645–13651.

[64] T. Suntola, Atomic layer epitaxy, Mater. Sci. Rep. 4 (1989) 261–312.

[65] S.M. George, Atomic layer deposition: an overview, Chem. Rev. 110 (2010) 111–131.

[66] M. Leskelä, M. Ritala, Atomic layer deposition (ALD): from precursors to thin film structures, Thin Solid Films 409 (2002) 138–146.

[67] R.W. Johnson, A. Hultqvist, S.F. Bent, A brief review of atomic layer deposition: from fundamentals to applications, Mater. Today 17 (2014) 236–246.

[68] N. Fairley, et al., Systematic and collaborative approach to problem solving using X-ray photoelectron spectroscopy, Appl. Surf. Sci. Adv. 5 (2021) 100112.

[69] J.G. Baker, J.R. Schneider, J.A. Raiford, C.D. Paula, S.F. Bent, Nucleation effects in the atomic layer deposition of nickel-aluminum oxide thin films, Chem. Mater. 32 (2020) 1925–1936.

[70] D. Jin, et al., Boosting photocatalytic performance for selective oxidation of biomass-derived pentoses and hexoses to lactic acid using hierarchically porous $Cu/Cu_2O/CuO$@CA, J. Mater. Chem. C Mater. 9 (2021) 16450–16458.

[71] T. Iivonen, et al., Low-temperature atomic layer deposition of copper(II) oxide thin films, J. Vac. Sci. Technol. A 34 (2016).

[72] X. Pang, et al., Annealing effects on microstructure and mechanical properties of chromium oxide coatings, Thin Solid Films 516 (2008) 4685–4689.

[73] B. Mandol, N. Mahuli, K. Ohno, L. Scudder, S.K. Sarkar, Atomic layer deposition of chromium oxide—An interplay between deposition and etching, J. Vac. Sci. Technol. A 39 (2021).

[74] H. Ekinci, et al., Effect of annealing on the structural, optical and surface properties of chromium oxide (Cr_2O_3) thin films deposited by e-beam evaporation for plasma etching applications, J. Alloys Compd. 875 (2021) 160087.

[75] F. Du, Q.-Y. Chen, Y.-H. Wang, Effect of annealing process on the heterostructure CuO/Cu_2O as a highly efficient photocathode for photoelectrochemical water reduction, J. Phys. Chem. Solid 104 (2017) 139–144.

[76] Y. Benrighi, et al., Characterization and application of the spinel $CuCr_2O_4$ synthesized by sol–gel method for sunset yellow photodegradation, J. Solgel Sci. Technol. 101 (2022) 390–400.
[77] G. Papadimitropoulos, N. Vourdas, V.E. Vamvakas, D. Davazoglou, Optical and structural properties of copper oxide thin films grown by oxidation of metal layers, Thin Solid Films 515 (2006) 2428–2432.
[78] A.M. Oje, A.A. Ogwu, A.I. Oje, An investigation of the work function and stability of chromium oxide thin films deposited by reactive magnetron sputtering, J. Appl. Electrochem. 52 (2022) 1551–1562.
[79] P. Qin, et al., Copper-doped chromium oxide hole-transporting layer for perovskite solar cells: interface engineering and performance improvement, Adv. Mater. Interf. 3 (2016).
[80] B.E. Davis, N.C. Strandwitz, Aluminum oxide passivating tunneling interlayers for molybdenum oxide hole-selective contacts, IEEE J. Photovolt. 10 (2020) 722–728.
[81] J. Dréon, et al., 23.5%-efficient silicon heterojunction silicon solar cell using molybdenum oxide as hole-selective contact, Nano Energy 70 (2020) 104495.
[82] L.G. Gerling, et al., Transition metal oxides as hole-selective contacts in silicon heterojunctions solar cells, Sol. Energy Mater. Sol. Cells 145 (2016) 109–115.
[83] L. Li, et al., Interfacial engineering of Cu_2O passivating contact for efficient crystalline silicon solar cells with an Al_2O_3 passivation layer, ACS Appl. Mater. Interf. 13 (2021) 28415–28423.